Electroosmotic Flow in Skin

A Summary to The Electrochemical Society for the 1998 Edward G. Weston Summer Research Fellowship

by Bradley D. Bath

Controlled-release drug delivery systems, employed in a variety of medical applications, are of increasing interest in the pharmaceutical and biomedical communities. One strategy involves the use of electricity to control and enhance the transport of therapeutic molecules across skin.[1] This method, referred to as iontophoretic transdermal drug delivery (TDD), has been successfully developed for the delivery of lidocain and fentanyl for local and systemic anesthetic administration,[2] and shows promise for the controlled delivery of numerous other drugs.

In iontophoretic TDD, the drug molecule is dissolved in a solution that is in contact with the skin. An electrical current is passed through the solution and skin, driving ions into the underlying skin tissues where they are transported by the circulatory system throughout the body. Recent studies have suggested that the transport of electrically neutral drug molecules across skin can also be enhanced by application of the electrical current.[3] This latter result suggests that iontophoretic TDD induces electroosmotic flow of solution across skin.[4] In the work described herein, scanning electrochemical microscopy (SECM) is used to directly observe and quantify electroosmotically-driven localized transport across skin. Previous studies using SECM have demonstrated that diffusion and migration of charged species across skin is localized to hair follicles.[5-6]

Figure 1 depicts the diffusion cell and SECM employed in the analysis of molecular transport across hairless mouse skin. The neutral redox-active permeant employed in this study, acetaminophen (AC), is dissolved in the solution on the donor side (bottom) of the skin. The permeant is allowed to freely diffuse across the skin; alternatively, the rate of transport may be varied by applying an iontophoretic current (i_{app}) between the two large Ag/AgCl electrodes placed on each side of the skin. As AC leaves the skin and emerges into the receptor compartment, it is electrochemically detected at the SECM tip via a two-electron oxidation reaction.[7]

As a model of a hair follicle in skin, thin sheets of mica containing a single pore filled with Nafion were synthesized, Fig. 2. Nafion is a permselective polymer that conducts ionic current exclusively by cation transport. The permselective nature of Nafion results in electroosmotic solution flow in the same direction as cation transport during iontophoresis.[8] In the experiments reported here, electroosmotic solution flow may be in the same or opposite direction as the diffusive transport of the neutral permeant, resulting in enhancement or diminishment of the overall flux. Hairless mouse skin, which has a net negative charge at physiological pHs, is reported to exhibit cation-selective properties.[9] When contacted with NaCl solutions, the transference number of Na^+ in skin has been measured to be approximately twice that of Cl^-.[9] It has been suggested that the permselective property of skin is due to a larger number of carboxylate ($-COO^-$) than ammonium ($-NH_3^+$) terminuses associated with protein amino acid residues.[10]

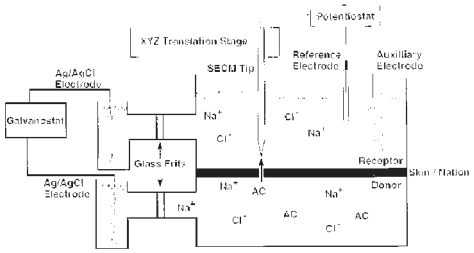

FIG. 1. Schematic of the SECM and iontophoresis cell used to investigate molecular transport of acetaminophen (AC) across Nafion and skin. AC is dissolved in solution in the lower (donor) compartment at a concentration ranging between 25 and 50 mM. Both the donor and receptor compartments contain 0.2 M NaCl. An iontophoretic current (i_{app}) is passed across the membranes using the galvanostat and two Ag/AgCl electrodes. AC is transported across the membrane by diffusion and electroosmotic flow. AC is electrochemically detected at the SECM tip as it emerges from the membrane into the receptor solution. The translation stage allows for positioning of the SECM tip in the x, y, and z dimensions with an accuracy of ~0.1 μm.

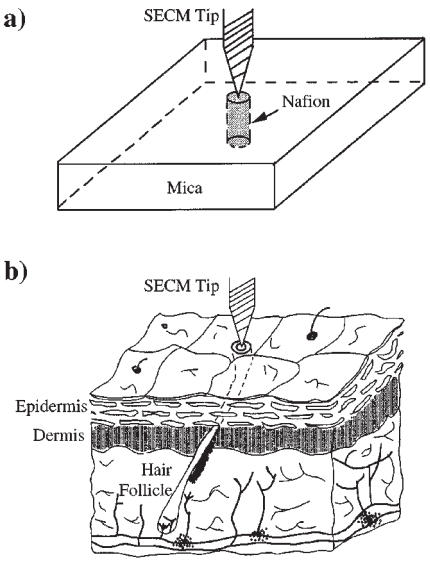

FIG. 2. Schematic of the SECM tip positioned directly above (a) a Nafion-filled pore in mica, and (b) a hair follicle in hairless mouse skin. The dimensions of the Nafion-filled pore (radius ~40 μm, length ~110 μm) are comparable to that of the hair follicle (radius ~20 μm, length ~500μm). The cation-selective properties of Nafion mimic the observed permselective properties of the hair follicle.

Figure 3 shows the voltammetric response of an SECM tip positioned directly above a Nafion-filled pore (top plot) and a hair follicle (bottom) under diffusive (i_{app} = 0 μA) and iontophoretic (i_{app} = 50 or -50 μA) conditions. A previously published theoretical analysis of this experiment demonstrates that the Faradaic current measured at the SECM tip is directly proportional to the rate of transport, Ω (mol/s), within the hair follicle or synthetic pore.[11] For example, when the tip is directly above the pore, the measured current is given by

$$i_t = (\pi n F r_t / 2a)\Omega \qquad [1]$$

where r_t is the tip radius, a is the radius of the pore or hair follicle, F is Faraday's constant, and n is the number of electrons transferred per AC molecule (= 2).

A qualitative comparison of the limiting currents in Fig. 3 suggests that the transport of AC in the Nafion-filled pore (a ≈ 40 μm) is remarkably similar to that of the hair follicle (a ≈ 20 μm). Using Eq. 1 and the voltammetric data corresponding to i_{app} = 0, the diffusive fluxes, N_{diff}, of AC in Nafion and the hair follicle are computed to be 8.1 x 10^{-10} and 3.3 x 10^{-10} mol/cm^{2}s, respectively.

When a positive current is applied (i_{app} = 50 μA, Fig. 3), the flux of AC dramatically increases across both the Nafion-filled pore and the hair follicle. Since AC is electrically neutral, the enhancement in flux must result from electroosmotic flow of solution through the pore and hair follicle. Na^+ is the

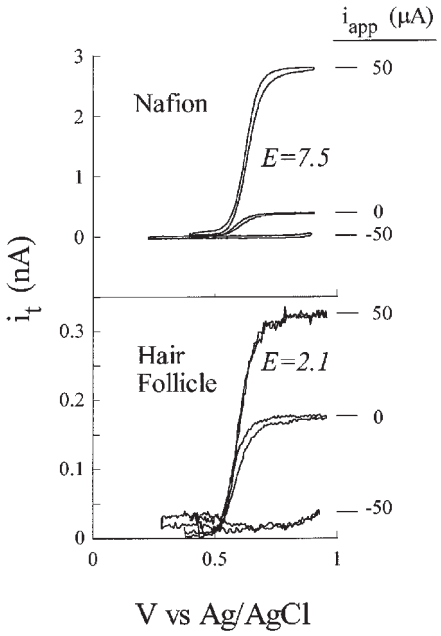

FIG. 3. Voltammetric response of a SECM tip positioned directly above a Nafion-filled pore (top) and above a hair follicle (bottom) as a function of iontophoretic current (i_{app} = -50, 0, 50 μA). The magnitude of the tip current is directly proportional to the flux of AC through the Nafion-filled pore or hair follicle, eq 1. The enhancement of the voltammetric current at positive iontophoretic current (i_{app} = 50 μA) is due to electroosmotic flow from the donor to receptor solution, in the same direction as molecular diffusion of AC. The decrease in voltammetric current at negative iontophoretic current (i_{app} = -50 μA) is due to electroosmotic flow from the receptor to donor solution, opposing the diffusive transport of AC. The enhancement factor, E, is the ratio of the flux of AC measured at i_{app} = 50 μA relative to the diffusive flux measured at i_{app} = 0 μA. E is a quantitative measure of the degree that electroosmotic flow enhances the flux of AC relative to diffusion.

predominant charge carrier in both structures (*vida supra*), and electroosmotic flow is anticipated to be in the same direction (from donor to receptor solution) as the diffusive flux of AC during positive iontophoretic current conditions. This prediction agrees with the observed enhancement in AC flux at i_{app} = 50 μA (N_{iont}). Using Eq. 1 and the voltammetric data in Fig. 3, N_{iont} is calculated to be 6.1 x 10^{-9} and 6.9 x 10^{-10} mol/cm^{2}s for the Nafion-filled pore and hair follicle, respectively. Conversely, when a negative current is applied, i_{app} = -50 μA (Fig. 3), the Na^+ flux and electroosmotic flow are from the receptor solution to the donor solution. Thus, electroosmotic flow opposes the diffusional flux of acetaminophen, resulting in a decrease in its net flux. The voltammetric data in Fig. 3 show that the acetaminophen flux is indeed reduced to background levels when electroosmotic flow is from the receptor to donor solutions.

The enhancement (E) in flux due to electroosmotic flow is described as the ratio of iontophoretic to diffusive flux[12] ($E = N_{iont}/N_{diff}$) computed to be 7.5 and 2.1 for Nafion and the hair follicle, respectively. E is a direct quantitative measure of the degree that electroosmotic flow enhances the flux of AC relative to diffusion. The larger value of E for Nafion is consistent with the higher degree of permselectivity towards cations of this material in comparison to skin.

For transport through the Nafion-filled pore, the experimental value of E can be used to determine the electroosmotic velocity υ_{eo} of AC. E is given by[12]

$$E=(\upsilon_{eo}l/D/\{1-\exp(-\upsilon_{eo}l/D)\} \qquad [2]$$

where l is the pore length (~500 μm for a hair follicle[13,14] and 110 μm for the Nafion-filled pore), and D is the diffusivity of AC in Nafion. The diffusivity of AC in Nafion has been experimentally determined to be 3.0 x 10^{-7} cm^2/s[15]. Substitution of this value, E = 7.7, and l = 110 μm into Eq. 2 yields υ_{eo} = 1.8 x 10^{-4}cm/s. At present, a similar analysis of υ_{eo} for transport in a hair follicle is prevented by a lack of knowledge of the diffusivity of AC in the hair follicle. ■

Acknowledgments

The author would like to thank The Electrochemical Society for the Summer Fellowship to support this research and ALZA Corp. for additional funding. The author also gratefully acknowledges Dr. Henry S. White and Dr. Erik R. Scott for their guidance.

References

1. A. K. Banga, *Electrically - Assisted Transdermal and Topical Drug Delivery*, Taylor and Francis, PA (1998).
2. S. Thysman, C. Tasset, and V. Preat, *Int. J. Pharm.*, **101**, 105 (1994).
3. M. J. Pikal, and S. Shah, *Pharm. Res.*, **7,** 213 (1990).
4. M. J. Pikal, *Adv. Drug Deliv. Rev.*, **9,** 201 (1992).
5. E. R. Scott, J. B. Phipps, and H. S. White, *J. Invest. Dermatol.*, **104,** 142 (1995).
6. E. R. Scott, H. S. White, and J. B. Phipps, *Solid State Ionics,* **53-56,** 176 (1992).
7. O. W. Lau, S. F. Luk, and Y. M. Cheung, *Analyst,* **114,** 1047 (1989).
8. R. Probstein, *Physicochemical Hydrodynamics,* Butterworths, New York (1992).
9. R. R. Burnette and B. Ongpipattanakul, *J. Pharm. Sci.*, **76,** 765 (1987).
10. G. Stutten, H. W. Spier, and G. Schwartz, *Handbuch Der Haut-und Geschlechtskrankheiten,* Sringer-Verlag, Berlin (1981).
11. B. D. Bath, R. D. Lee, H. S. White, and E. R. Scott, *Anal. Chem*. **70,** 1047 (1998).
12. V. Srinivasan and W. I. Higuchi, *Int. J. Pharm.*, **60,** 133 (1990).
13. R. L. Bronaugh, R. F. Stewart, and E. R. Congdon, *Toxicol. Appl. Pharmacol.*, **62,** 481 (1982).
14. A length of 500 μm for the hair follicle assumes that molecular transport occurs across the epithelial cells lining the follicle around its bulb (Fig. 2) imbedded in the dermis. Once AC has traversed the follicle wall, it is transported throughout the inside of the follicle until it reaches the receptor compartment (l≈500μm).
15. B. D. Bath, *unpublished results*, University of Utah (1998).

About the Author

Bradley Bath *is a fourth year graduate student at the University of Utah working in Dr. Henry S. White's research group. Bath's research interests currently include applied electrochemical techniques, controlled release drug delivery systems, and pharmaceutical drug development.*

Pattern-Dependent Charging Damage in High Density Plasma Processes

A Summary Report to The Electrochemical Society for the 1998 Colin Garfield Fink Summer Research Fellowship

by Gyeong Soon Hwang

Charging damage caused by electron shading during high-density plasma processing has emerged as a serious issue in semiconductor device fabrication. It manifests itself into two ways: (1) lateral sidewall etching, so called notching,[1] and (2) gate oxide degradation.[2] While the physics of the notching effect is rather well understood,[3] the latter damage behavior has not been clearly elucidated.[4] Gate oxide degradation is commonly attributed to Fowler-Nordheim tunneling currents brought about by a strong electric field across the thin oxide. By undermining device performance and reliability, plasma-induced charging damage becomes more critical as device dimensions shrink and the number of plasma processing steps increases.

The electron shading effect takes place when a patterned wafer is exposed to a plasma due to the directionality difference between ions and electrons arriving at the wafer even when the plasma is uniform. High-aspect-ratio photoresist patterns on poly-Si or metal gates hinder the less anisotropic electrons from reaching the gates, while the directional ions are barely influenced by the patterns, as shown in Fig. 1. During over-etching, the ion and electron current imbalance causes the potential of the poly-Si or metal gate connected to the gate oxide to rise which, in turn, induces a potential drop across the oxide and subsequent tunneling currents flowing through it. In light of the mechanism, the electron-shading induced charging damage is likely to be inherent to high density plasma processing. Thus far, several ways have been suggested to alleviate the charging problem by manipulating plasma parameters and substrate bias conditions.[5] However, the actual effects are still under debate, mainly due to the difficulty in precisely monitoring the ion dynamics inside submicron patterns. Moreover physical models capable of addressing explicitly the plasma-surface interactions are currently inadequate. This situation necessitates the development of a robust microstructure charging model and related simulation techniques.

We have developed a Monte Carlo (MC) based simulation model that combines plasma discharge, sheath dynamics, charged particle dynamics, and microstructure charging dynamics

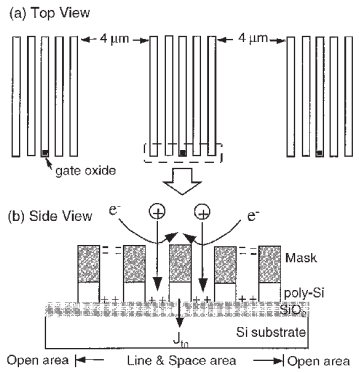

FIG. 1. Schematic of the line and space patterns used for the simulation and the electron shading model.

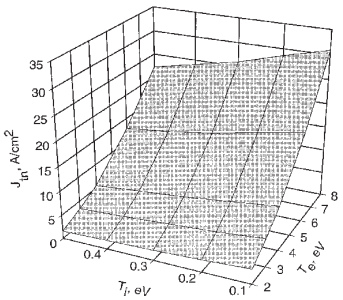

FIG. 2. Tunneling current (J_{tn}) flowing through the gate oxide as a function of the ion temperature (T_i) and the electron temperature (T_e).

such as charge transfer, surface current, stress induced tunneling, and so forth. The numerical study has demonstrated that oxide damage is a rather complex function of plasma properties, pattern configuration, and rf substrate bias conditions.[6] We address here the ion and electron temperature dependence. Low-pressure high-density (LPHD) plasma tools, recently widely used because of their high fidelity pattern transfer capabilities, usually exhibit high ion and electron temperatures: T_i = 0.1-0.5 eV and T_e = 3-6 eV. While it is well known that the charging-induced damage worsens with increasing electron temperature,[5] the reason is not clearly understood and no quantitative model exists to predict the electron temperature dependence. Moreover, to the best of our knowledge, the influence of the ion temperature has not been investigated, despite possible contributions to charging damage.

For the present simulation, low-pressure high-density chlorine plasma conditions are assumed: 100% dissociation of a Cl_2 plasma with density of 10^{12} cm^{-3} at pressures lower than 5 mTorr. The substrate is biased at 0.4 MHz with a peak-to-peak voltage of 60 V. The angular and energy distributions of ions and electrons arriving at the substrate are calculated by MC techniques based on nonlinear sheath theory.[7] The line and space (L&S) pattern consists of five 0.3 μm lines separated by 0.3 μm spaces, as shown in Fig. 1. Each line consists of 0.6 μm thick photoresist onto 0.3 μm thick poly-Si. The distance between two patterns is 4 μm. The center poly-Si line is connected to a thin gate oxide with a thickness of 4 nm. The Si substrate is taken to be grounded. Surface currents are allowed to flow when a surface electric field exceeds 1 MV/cm on the SiO_2 and photoresist surfaces. Here, the antenna area ratio (AAR), which is defined as the area ratio of a poly-Si bottom to the gate oxide, is held constant at 1,000.

In Fig. 2, the steady-state tunneling current density (J_{tn}) flowing through the gate oxide is presented as a function of the electron temperature (T_e) and the ion temperature (T_i). The tunneling current density increases with T_e at constant T_i, which is consistent with experimental results reported in the literature.[5] Interestingly, the results also demonstrate that the tunneling current is strongly dependent on T_i as well; at T_e = 2 eV, the current density is reduced by almost 50% as T_i rises from 0.1 to 0.5 eV. Considering that the oxide damage is proportional to the total tunneling current, this result indicates that the gate oxide shall be less damaged at lower T_e and higher T_i. To gain better understanding of the damage behavior, the potential distribution developed over the L&S pattern is plotted for three different sets of the ion and electron temperatures, as shown in Fig. 3. As a result of the ion and electron current imbalance at the initial stage of charging, the trench bottom accumulates positive charge, thereby increasing the bottom potential until it reaches steady state by repelling incoming ions and attracting more electrons. Under the plasma and rf bias conditions considered here, the ion energy distribution function (IEDF) exhibits a bimodality that peaks at V_L (= $T_e/2 + V_{min}$) and V_H (= $T_e/2 + V_{min} + V_{pp}$), where V_{pp} is the peak-to-peak potential and V_{min} is the dc minimum sheath potential. The V_{min} is a function of T_e; V_{min} is approximately 5 and 20 V for T_e of 2 and 8 eV, respectively.[8] The

low energy ions are deflected by the high bottom potential and may return to the upper mask sidewalls to neutralize the region which is typically charged negatively by direct electron irradiation. The high bottom potential may also weaken directly the negative entrance potential, thereby increasing the electron supply. To reflect enough low energy ions, the bottom potential should be higher than the V_L, which indicates that the potential of the trench bottom may be a function of T_e. Apparently, the bottom potentials at T_e = 8 eV (Fig. 3(a)) are significantly larger than that at T_e = 2 eV (Fig. 3(b)), except for the center poly-Si line whose potential is primarily determined by the gate oxide thickness. More negative entrance potential at T_e = 8 eV (a consequence of more energetic electron bombardment) weakly affects the electron flux into the trench because of the relatively larger population of high energy electrons. This implies that the relative net ion flux into the trenches is nearly independent of T_e. Then, it becomes evident that the difference in local electric fields of the lower trench region is mainly responsible for the drastic change of the tunneling current. More asymmetric potential distributions at T_e = 8 eV tend to push more ions and fewer electrons to the sidewalls of the center line, thereby increasing the net ion current there. The larger potential drop along the SiO_2 surface at the trench bottom also leads to larger surface ion currents to the center poly-Si. Along with the local electric field effects, the larger T_e sustains a larger plasma conduction current; that is, $\langle J_i \rangle = \langle J_e \rangle = 0.61\, n_o (k_b T_e / m_i)^{1/2}$, where $\langle J_i \rangle$ and $\langle J_e \rangle$ are the period averaged ion and electron conduction currents onto a wafer, respectively, n_o is the plasma density, k_b is the Boltzmann constant, and m_i is the ion mass. As a result, the tunneling current increases with increasing T_e.

A comparison of Fig. 3b and 3c shows the ion temperature effect. As T_i increases, the ion angular distribution becomes broader, thereby directly reducing the negative entrance potential further. As a result, more electrons can flow into the trenches, ultimately reducing the tunneling current. Note that while the ion and electron temperature dependence is more or less sensitive to the pattern configuration, the general trend remains unchanged: the charging damage is reduced by decreasing T_e and/or increasing T_i.

While experiments are limited because of difficulties in precisely monitoring the complex dynamics of plasma-surface interactions occurring inside submicron patterns, the numerical model has provided significant insights into the pattern-dependent charging damage. Since electron shading is rather inherent to plasma processing, better understanding of the influence of processing conditions is crucial to minimize its impact on future generations of IC devices. ■

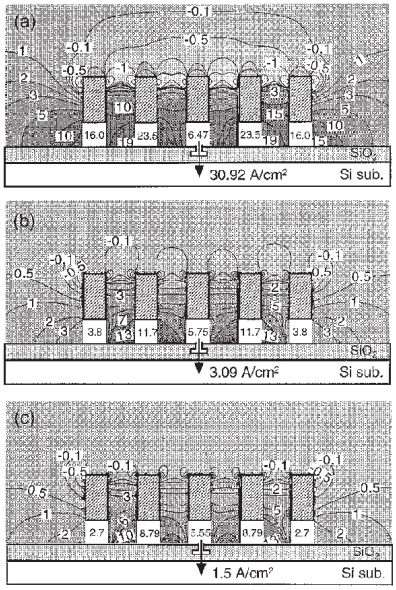

Fig. 3. Steady-state charging potential contour map for three different sets of the ion and electron temperatures: (a) T_i = 0.1 and T_e = 8 eV, (b) T_i = 0.1 and T_e = 2 eV, and (c) T_i = 0.5 and T_e = 2 eV.

References

1. T. Nozawa, T. Kinoshita, T. Nishizuka, A. Narai, T. Inoue, and A. Nakaue, *Jpn. J. Appl. Phys.*, **34**, 2107 (1995).
2. K. Hashimoto, *Jpn. J. Appl. Phys.*, **33**, 6013 (1994).
3. G. S. Hwang and K. P. Giapis, *J. Vac. Sci. Technol.* B, **15**, 70 (1997).
4. K. Hashimoto, F. Shimpuku, A. Hasegawa, Y. Hikosaka, and M. Nakamura, *Thin Solid Films*, **316**, 1 (1998).
5. T. Kamata and H. Arimoto, *J. Appl. Phys.*, **80**, 2637 (1996).
7. G. S. Hwang and K. P. Giapis, *to be submitted.*
8. M. A. Lieberman, *IEEE Trans. Plasma Sci.*, **16**, 638 (1988).
9. M. A. Lieberman and A. J. Lichtenberg, *Principles of Plasma Discharges and Materials Processing*, Wiley-Interscience, New York, p. 366 (1994).

About the Author

Gyeong S. Hwang *works as a research assistant with Professor K. P. Giapis in the Chemical Engineering Department at California Institute of Technology.*

Electron-Transfer Kinetics of Ferrocene in Phenyl Containing Monolayers

A Summary Report to The Electrochemical Society for the 1998 Joseph W. Richards Summer Research Fellowship

by James J. Sumner

Electron-transfer kinetics have been studied in recent years for application to many fields, including chemistry (photochemistry and electrochemical sciences)[1-2], biology (photosynthesis and respiration),[3] and materials science and technology (sensors and molecular scale electronics)[4]. Monolayer systems have been an effective way to probe electron-transfer kinetics.[5-7] Electrochemical studies of monolayers have given information on electronic conjugation and its effect on electron-transfer rates. The focus of work has been to synthesize two new molecules which will show the effect of adding electronic conjugation in bridges connecting a redox active group to an electrode on electron-transfer kinetics in monolayers.

The model molecule of this study was 4-(9-mercaptononoxyl) phenylferrocene (compound 1). The 4-hydroxy(phenylferrocene) was prepared using diazonium chemistry from ferrocene and 1,4-aminophenol. The alkane chain was added to the hydroxyl using Williamson ether synthesis with dibromononane and a conversion of bromide to a thiol was achieved using thiourea.

The goal of synthesizing the 1,3 analogue of compound 1 was not achieved. The synthesis of 3-hydroxy(phenylferrocene) from diazonium chemistry directly proved to be impractical due to rearrangement to the 1,4 orientation. It was found that a meta-directing substituent was necessary to achieve a 1,3 substitution pattern. Nitro was selected as the substituent to insure no conversion to the 1,4 the 3-nitro(phenylferrocene) was easily synthesized in large yields. Conversion of the nitro to the alcohol and continuation of the synthesis is the next step in obtaining the final product. Investigating meta-directing protecting groups for alcohols may also be advantageous to reduce the number of steps in the synthesis.

Ferrocenyl-alkanethiols were also used. These had no conjugation in the bridge between the ferrocene and the electrode. Three alkane chain lengths, n = 11, 12, and 16, were available from a previous study.

Compound 1 was first studied using fast scan cyclic voltammetry.[5] A rate constant of k_0 ~1100 s^{-1} was obtained. Monolayers of this molecule were then studied using ac voltammetry with two different data analysis procedures based on equivalent circuits. One procedure utilized the complex-plane data presentation with ZPlot software (Scribner Associates, Inc.) and the other utilized a technique of simulating the ratio of peak current to background current versus frequency using Laviron equations.[8] The complex-plane analysis gave a k_0 ~1500 s^{-1} and the ratio analysis gave a k_0 ~2200 s^{-1}.

The rate constant was higher for monolayers with a phenyl group in the bridge between the ferrocene and the electrode by almost an order of magnitude in comparison to a bridge of a non-conjugated alkane chain with the same number of bonds (fourteen) in the bridge between the ferrocene and the electrode. This was shown by obtaining voltammetric data on the ferrocenyl-alkanethiol monolayers of varying chain length and plotting the natural log of k_0 versus the number of bonds. Figure 1 shows the data for monolayers of the three representative ferrocenyl-alkanethiols. This plot yields a fairly straight line with a slope of -1.0 per CH_2. Interpolating the alkane data in Fig. 1 for a fourteen carbon chain yields k_0 ~ 190 s^{-1} approximately an order of magnitude less than the value obtained for compound 1.

A comparison of electronic coupling of 1,4 and 1,3 linkages would not be made at present because of difficulties in the synthesis of the 1,3 analogue. The increased electron-transfer rate by inclusion of a conjugated bridging group was confirmed by AC voltammetry and fast scan cyclic voltammetry. ■

References

1. J. Mattay, *Photoinduced Electron Transfer V*, Vol. 168, Springer Verlag, Berlin (1993).
2. I. Rubenstein, *Physical Electrochemistry: Principles, Methods, and Applications*, Marcel Dekker, New York (1995).
3. G. McLendon, *Acc. Chem. Res.*, **21**, 160, (1988).
4. C. A. Mirkin and M. A. Ratner, *Ann. Rev. Phys. Chem.*, **43**, 719 (1992).
5. K. S. Weber and S. E. Creager, *Anal. Chem.*, **66**, 3164 (1994).
6. C. E. D. Chidsey, *Science*, **251,** 919 (1991).
7. L. Tender, M. T. Cater, and R. W. Murray, *Anal. Chem.*, **66,** 3171 (1994).
8. E. Laviron, *J. Electroanal. Chem.*, **97,** 135 (1979).

About the Author

James Sumner *is a fourth year graduate student under the direction of Dr. S. E. Creager at Clemson University.*

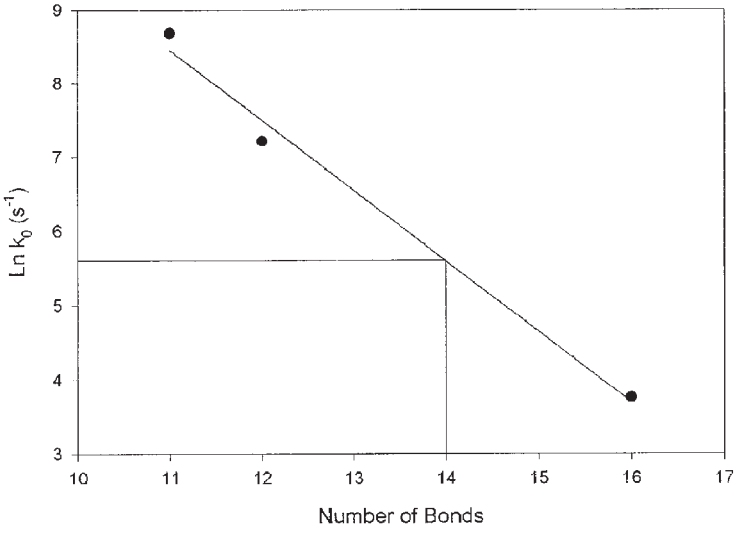

FIG. 1. Plot of ln k_0 versus number of bonds in the bridge of the alkane ferrocene. Linear regression yields a R^2 = 0.989 and a k_0~190 s^{-1} for a bridge chain length of fourteen carbons.

Catalysts Based on Dendrimer-Encapsulated Noble Metal Nanoclusters

A Summary Report to The Electrochemical Society for a 1998 Department of Energy Summer Research Fellowship

by Minqgi Zhao

Catalysis and electrocatalysis provide key applications for noble-metal nanoclusters.[1,2] Synthetic routes to metal nanoparticles include evaporation and condensation, and chemical or electrochemical reduction of metal salts in the presence of stabilizers.[1] The purpose of the stabilizers is to control particle size and prevent agglomeration. However, stabilizers also passivate cluster surfaces. For some purposes, such as catalysis, it is desirable to prepare small, stable, but not-fully-passivated particles so that substrates can access the encapsulated clusters.

In this report, we demonstrate a general template-based method for preparing monodisperse metal nanoclusters suitable for catalysis (Fig. 1). Our approach involves the use of hydroxyl-terminated polyamidoamine (PAMAM) Starburst dendrimers (Gn-OH, where n is the generation) as both template and stabilizer. These dendrimers are monodisperse, hyperbranched polymers, which are roughly spherical in shape, highly functionalized, sterically crowded on the exterior, and somewhat hollow on the interior.[3] The molecular weight, size, and the steric crowding on the exterior of a dendrimer are dependent on the dendrimer generation: the larger the generation, the higher the molecular weight, and the more crowding on the dendrimer surface. A schematic illustration of a hydroxyl-terminated fourth-generation PAMAM dendrimer is shown in Fig. 1. By using dendrimers as both monodisperse templates and stabilizers, we achieve particle stability and full control over particle size, while simultaneously allowing substrates to penetrate the dendrimer interior and access the cluster surface.

Our approach for preparing dendrimer-encapsulated metal particles has been described previously.[4] First metal ions are extracted into the interior of a Gn-OH dendrimer and then the trapped metal ions are chemically reduced to yield dendrimer-encapsulated zero-valent metal particles. Many transition-metal ions, including Cu^{2+}, Pt^{2+}, Pd^{2+}, Ru^{3+}, and Ni^{2+}, partition into the interior of PAMAM dendrimers where they are strongly complexed by interior tertiary amine functional groups. Here we focus on the preparation of Pt and Pd nanoclusters within dendrimers. The number of complexed metal ions per dendrimer can be nearly monodisperse. Thus, by preloading a dendrimer "nanotemplate" with $PtCl_4^{2-}$ or $PdCl_4^{2-}$ and then chemically reducing this composite in situ with BH_4^-, a dendrimer-encapsulated Pt or Pd cluster containing the same number of atoms results.[5,6] For example, we can prepare intradendrimer clusters containing between 12 and 60 Pt atoms ($G4\text{-}OH(Pt_n)$) or 12 and 40 Pd atoms ($G4\text{-}OH(Pd_n)$). The successful preparation of monodisperse dendrimer-encapsulated metal nanoparticles is dependent on the chemical structure of the dendrimer host. For example, amine-terminated dendrimers (G4-NH_2) are not suitable for this purpose because the metal ions bind to the terminal primary amine groups, as well as the interior tertiary amines, and a dark precipitate of bulk metal is observed upon reduction. This is a consequence of agglomeration of the unprotected metal clusters coordinated to the dendrimer exterior.

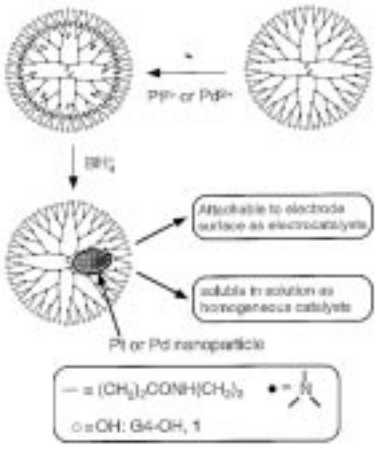

FIG. 1. Schematic illustration of hydroxyl-terminated, fourth-generation PAMAM dendrimers (G4-OH), synthesis of Pt or Pd nanoparticles within the dendrimer template, and the use of the composites as catalysts. Between 12 and 60 Pt^{2+} ions or 12 and 40 Pd^{2+} ions can be loaded into a single dendrimer and, upon reduction with BH_4^-, an entrapped cluster containing the same number of atoms results.

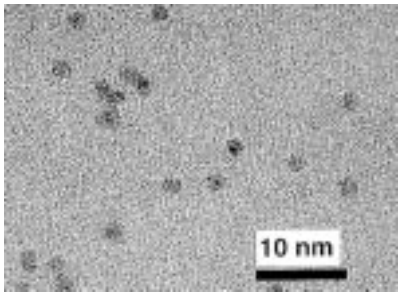

FIG. 2. HRTEM image of $G4\text{-}OH(Pt_{60})$ showing the nearly monodisperse size and shape distribution. The average size for these particles is 1.6 nm.

Electron microscopy confirms that chemical reduction of dendrimer-Pt^{2+} complexes ($G4\text{-}OH(Pt^{2+})_n$) and dendrimer-Pd^{2+} complexes ($G4\text{-}OH(Pd^{2+})_n$) yields intradendrimer metal nanoparticles. The micrographs indicate that the particles are nearly monodisperse and that their shape is roughly spherical. For $G4\text{-}OH(Pt_{40})$, $G4\text{-}OH(Pt_{60})$, and $G4\text{-}OH(Pd_{40})$ particles, the cluster diameters are estimated to be 1.4 ± 0.2, 1.6 ± 0.2, and 1.3 ± 0.3 nm, respectively. Figure 2 shows a TEM image of $G4\text{-}OH(Pt_{60})$. Chemical reduction of Pt^{2+} salts in the presence of ligands or polymers usually produces irregularly shaped particles having a broad size distribution.[7] Therefore, the results presented here are significant: we can prepare monodisperse nanoparticles and control the size of the particles by using dendrimers as both template and stabilizer.

Dendrimer-encapsulated Pt and Pd particles are stable for more than four months, can be isolated in dry form, and can be redissolved. We have shown these materials have applications as both heterogeneous and homogeneous catalysts. For example, a Au/$G4\text{-}OH(Pt_{60})$-modified electrode shows high electrocatalytic activity for O_2 reduction.[5] Soluble dendrimer-encapsulated Pt or Pd particles can catalyze the hydrogenation reaction of allyl alcohol and N-isopropyl acrylamide in water.[6] Additionally, the dendrimer acts as a "nanofilter" which shows preferential reduction of the linear alkene.

In summary, dendrimers have been shown to act as templates and stabilizers for preparing monodisperse precious-metal nanoclusters. The size of the nanoclusters depends on the type and generation of the dendrimer and the number of metal ions preloaded into the dendrimer interior prior to reduction. These dendrimer-encapsulated Pt or Pd nanoparticles can be immobilized to electrode surfaces or used in bulk solution for heterogeneous or homogeneous catalysis, respectively. ■

Acknowledgments

The author would like to thank Professor Richard M. Crooks for his guidance in this project. The financial support of The Electrochemical Society and the National Science Foundation (CHE-931344) is also gratefully acknowledged.

References

1. G. Schmid, Ed.; Clusters and Colliods: From Theory to Applications; VCH, Weinheim (1994).
2. G. J. K. Acres and G. A. Hards; *Phil. Trans. R. Soc. Lond. A.*, **354**, 1671 (1996).
3. O. A. Mattews, A. N. Shipway and J. F. Stoddart; *Prog. Polym. Sci.*, **23**, 1 (1998).
4. M. Zhao, L. Sun, and R. M. Crooks; *J. Am. Chem. Soc.*, **120**, 4877 (1998).
5. M. Zhao and R. M. Crooks; *Adv. Mater.*, in press.
6. M. Zhao and R. M. Crooks; *Angew. Chem. Int. Ed. Engl.*, in press.
7. G. Schemid, *Chem. Rev.*, **92,** 1709 (1992).

About the Author

Mingqi Zhao *is a graduate student in the Department of Chemistry at Texas A&M University, College Station, TX. His research interests include nanoparticles, catalysis and organic thin films.*